MSA UNIVERSITY ENGINEERING JOURNAL

Behavior of Piles Reinforced by Geosynthetics Under Lateral Load

Abstract

This paper introduces the results of eleven lateral pile loading tests performed on concrete piles reinforced with different materials such as FRP bars, geosynthetics geogrids, and composite of two materials to check their efficiency in carrying the lateral load. The lateral loading pile test was applied on three groups consisting of ten reinforced concrete pile specimens, and control concrete pile specimen reinforced by steel bars. All samples have the same dimensions (150 mm diameter x 1050 mm length). This research assumed that the pile was placed in a very soft clay soil and rested on a crushed stone layer, so the frictional effect of the soil was neglected. A comparison has been carried out between experimental results for all samples. The experimental results illustrated that the lateral loads carried by piles were increased up to 25.3% by using FRP bars, biaxial geogrid, and uniaxial geogrid. Moreover, a non-linear finite element analysis was verified by Abaqus standard software and achieved a great rapprochement with the experimental results. Finally, a comparison was carried out between the reinforcement cost for all samples which showed that using these composite piles decreased its cost up to 59%.

Keywords: Geosynthetics Geogrid, Piles, Composite piles, Lateral load.

ENGINEERING JOURNAL Volume 2 Issue 2
Received Date January 2023
Accepted Date March 2023
Published Date March 2023
DOI: 10.21608/MSAENG.2023.291910

1. Introduction

Previously, pile foundations are usually constructed by using accustomed materials or combinations of materials: Steel, concrete, also wood. However, when used in tough conditions like riverfront areas or polluted soil conditions, these materials pose a variety of difficulties [1] such as steel corrosion, wood damage, and the deterioration of RC piles in deep foundations [2]. To address these negative effects, researchers have examined the use of renewable materials as piling alternatives, such as glass or carbon fiber composites [3-6]. The use of fiber-reinforced polymer (FRP) bars and geosynthetic geogrids (G) as pile reinforcement materials was discovered to be a promising strategy, due to their high strength-weight ratio, durability, and high ability to anti-corrosion [7][8]. Composite piles are commonly used as waterfront barriers, fenders, and bearing piles for light structures in ports due to the ongoing creation of novel composite materials [9-13]. They were also used in bridge rehabilitation work as load-bearing substructures [14]. Most recently, they were utilized in a timber pile replacement job. [15] and as a support in shoring-up boardwalks [16]. Aside from these few uses, composite piles haven't been widely used yet due to the lack of installation guidelines [13]. The results of a series of small-scale static axial and lateral pile load experiments conducted on model Fiber Reinforced Polymer (FRP) piles and steel piles were presented by Giraldo J. et al. in 2014. They produced hollow FRP piles utilising carbon and glass fibres with varying orientations. They demonstrated that the axial bearing capacity of FRP piles is 5–40% greater than that of steel piles. In the presence of lateral loads, the FRP foundations exhibited greater deflections than their steel counterparts. According to the results they presented, FRP piles have the necessary properties to serve as load-bearing members based on axial geotechnical capacity [17]. Ali A. H. et al. conducted a numerical analysis, employing the finite element model (FEM) and modified compression field theory (MCFT), to evaluate the shear capacity and behaviour of circular concrete piles reinforced with steel and FRP bars, taking into account shear behaviour, shear strength, and deflection shape. The FEM and MCFT models were validated against the experimental results of previously tested full-scale circular concrete specimens. The predicted load-deformation response curve and load-strain curve for reinforced concrete and reinforcing bars were compared to experimental results. The FEM results demonstrated that the model accurately predicted the behaviour of the specimens. While the Response 2000 (R2K) software and the modified compression field theory provided accurate predictions of the shear strength [18]. Up to now, Egyptain Code Practice 201 (201) [19] lack theories for using glass fiber bars GFRP, carbon fiber bars CFRP, or geosynthetic geogrids in reinforcing piles.

This study aims to investigate the behavior of using different materials in pile reinforcement and check their efficiency in carrying the lateral load. Lateral pile loading tests were applied on eleven piles as a concrete pile reinforced with glass fiber reinforced polymer bars, concrete pile reinforced by carbon fiber reinforced polymer bars, concrete pile reinforced by triaxial geosynthetics geogrids, biaxial geosynthetics geogrid, or uniaxial geosynthetics geogrid, concrete pile reinforced by triaxial, biaxial, or uniaxial geosynthetics geogrids with a steel bar in the middle of core, and control concrete pile (Ps) reinforced by steel. Also, the reinforcing costs for all samples were estimated. The variables of the test program were the materials used in the reinforcement and identified by letter code as follows:

Steel (s), GFRP bars (l), CFRP bars (c), Geosynthetic geogrids (triaxial (GA) (GB), biaxial (GC), uniaxial (GD)).

2. Experimental Program

2.1. Samples and Test Matrix

Eleven samples are included in the experimental program as shown in table (1). Three groups of pile specimens were constructed and tested. Each group contains reinforced concrete piles with dimensions (150 mm diameter x 1050 mm length). All samples have the same dimensions and approximately the ratio of reinforcement. The control pile sample is reinforced using high tensile steel formed of four bars with 8 mm diameter and a spiral stirrup of mild steel with 6 mm diameter. The first group consisted of two pile specimens (Pl, Pc) were reinforced using GFRP bars or CFRP bars formed of four bars with 8 mm diameter and a spiral stirrup of mild steel with 6 mm diameter. The second group consisted of four pile specimens (PGA, PGB, PGC, and PGD) were reinforced using GA, GB, GC, or GD formed as a cylindrical shell. The third group consisted of four pile specimens (PsGA, PsGB, PsGC, and PsGD) were reinforced using GA, GB, GC, or GD formed as a cylindrical shell and steel bar with 12 mm diameter in the middle of core. The reinforcing schemes used in the present study according to the previous explanation was shown in fig. 1. The variable of the test program is the materials used in the reinforcement and identified by letter code as follows: Steel (s), GFRP bar (l), CFRP bar (c), triaxial geosynthetics geogrids TX130 (GA), triaxial geosynthetics geogrid TX150 (GB), biaxial geosynthetics geogrids DBG30 (GC), and uniaxial geosynthetics geogrid HDPE (GD).

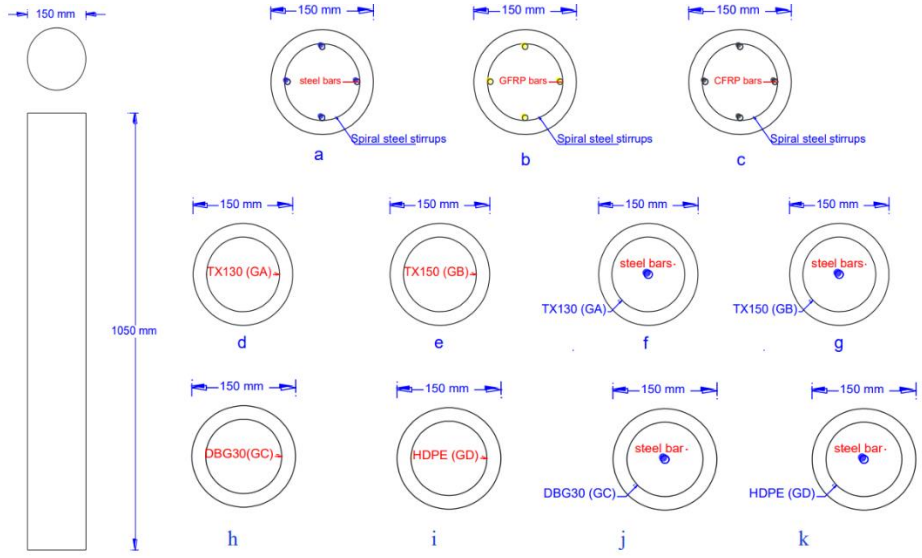

Fig. 1. Cross section of composite piles. (a) control pile Ps, (b) Pl, (c) Pc, (d) PGA, (e) PGB, (f) PsGA, (g) PsGB, (h) PGC, (i) PGD, (j) PsGC, and (k) PsGD.

Table 1. Test matrix.

Group No.	Pile Code	Applied Material	Reinforcement (A_S/A_C) %
Reference	Ps	Steel Rft. (s)	1.13
First Group	Pl	Glass Fiber bars (l).	1.13
	Pc	Carbon Fiber bars (c).	1.13
Second Group	PGA	Geogrid TX130 (GA)	1.13
	PGB	Geogrid TX150 (GB)	1.15
	PGC	Biaxial Geogrid (DBG30) (GC)	1.13
	PGD	Uniaxial Geogrid (HDPE) (GD)	1.13
Third Group	PsGA	Steel Bar (S)+ Triaxial Geogrid (GA)	1.13+0.64
	PsGB	Steel Bars (S) + Triaxial Geogrid (GB)	1.15+0.64
	PsGC	Steel Bars (S) + Biaxial Geogrid (GC)	1.13+0.64
	PsGD	Steel Bars (S) + Uniaxial Geogrid (GD)	1.13+0.64

Material Properties

Ordinary Portland Cement (OPC-42.5 grade), and natural sand with 2.6 fineness moduli with filter stones having a maximum aggregate size of 9 mm were used in the tested specimens. At 28 days, the predicted compressive strength (fcu) was 20 MPa. The actual fcu was gained on the day of testing.

High tensile steel bars grade (40) that have a yield stress of 40 Ksi with 8 mm diameters was used as the main reinforcement of the tested piles. Normal mild steel bars grade (36) that have a yield stress of 36 Ksi was used for spiral stirrups 6 mm diameter. The reference concrete piles were reinforced with 6 mm diameter normal mild steel as spiral stirrups and 8 mm diameter high tensile steel bars as main reinforcement.

GFRP bars used in this research were manufactured by Russian company Armastek and imported by Fiber Reinforcement Industries Company [20]. The mechanical properties of the GFRP bars were given in Table 2, according to the manufacturer. The GFRP bars were used 8, 12 mm in diameter as shown in fig. 2a. CFRP bars used in this research were manufactured from SikaWrap230, which is a product of Sika Company [21]. The bars used were made from strips of CFRPs rolled and bonded using epoxy Sikadur-330 then put in a mold, a resin was cast and let till hardened. The mechanical properties of the CFRP were given Table 2, in accordance with the manufacturer. The CFRP bars were used 8, 12 mm in diameter as shown in fig. 2b.

Triaxial geosynthetics Geogrid manufactured by Tensar International Corporation and imported by National Geotechnical Company for (GEOTECH) [22]. Table 2 gives the mechanical properties of geogrid, according to the manufacturer. Geosynthetics geogrids TX130 (GA) and TX150 (GB) were used as shown in Fig. 2c. and Fig. 2d. respectively.

Biaxial geosynthetics geogrids were used in this study manufactured by Degla Group for Synthetics Fibers & Plastic. [23] The mechanical properties of Biaxial geogrids were given Table 2, in accordance with the manufacturer. Biaxial Geogrids DBG30 were used as shown in fig. 2e. Tensile strength and elongation were tested with standards of EN ISO 10319 & ASTM D6637 & GG2-87.

Uniaxial geosynthetics geogrids were used in this study manufactured by Degla Group for Synthetics Fibers & Plastic. [23] The mechanical properties of uniaxial geogrids were given Table 2, in accordance with the manufacturer. Uniaxial Geogrids DBG30 were used as shown in fig. 2f. Tensile strength and elongation were tested with standards of EN ISO 10319 & ASTM D6637 & GG2-87.

Table 2. Dimensions and characteristic properties of FRP bars. [20],[21],[22], [23].

Characteristics	**CFRP bar**	**Characteristics**	**GFRP bar**
Diameter (mm)	8	Diameter (mm)	8
Tensile strength (MPa)	1050	Tensile strength (MPa)	630
Modulus of elasticity (MPa)	120000	Modulus of elasticity (MPa)	28570
Strain at failure	0.5%	Strain at failure	2.2%
Characteristics	**Geogrid**	**Characteristics**	**Geogrid**
Thickness (mm)	1.3	thickness (mm)	1.5
Tensile strength (N/mm)	10	Tensile strength (N/mm)	11.25
Modulus of elasticity (MPa)	200000	Modulus of elasticity (MPa)	225000
Strain at failure	0.5%	Strain at failure	0.5%
Characteristics	**Geogrid**	**Characteristics**	**Geogrid**
Aperture Dimensions (mm)	3.2	thickness (mm)	5
Rib Thickness (mm)	3.2	Tensile strength (N/mm)	45
Tensile strength (N/mm)	30	Long-term strength (N/mm)	21.12
Elongation (%)	11%	Elongation (%)	5%

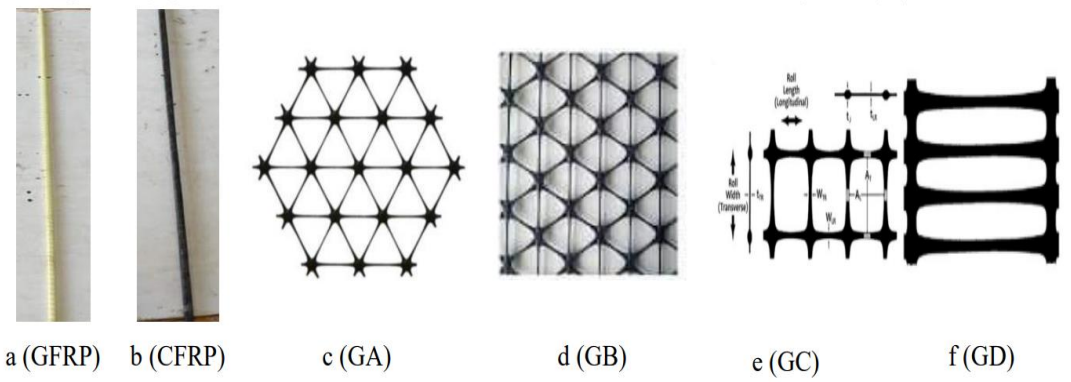

Fig. 2. The material types.

2.2. Test Set-Up and Instrumentations

The samples were loaded with a hydraulic jack with a maximum capacity of 1000 (KN), linked to electric pump, and hung with a rigid reaction frame with a maximum capacity of 1000 (KN). The samples were simply placed on two I beams at both sides; one beam represented the pile cap and the other represented the end bearing layer. The load was transferred laterally by a steel bar to the pile surface using steel plate. The applied lateral load was measured with a load cell with a maximum capacity of 1000 (KN) placed beneath the hydraulic jack. Only one Linear Variable Differential Transducer (LVDT) was installed beneath the upper third of the pile surface to monitor displacement. All test data were collected with a data acquisition system and collected on a computer at two-second intervals. Figure 3 depicts the test setup which was applied in the concrete laboratory of Benha Faculty of Engineering at the University of Benha.

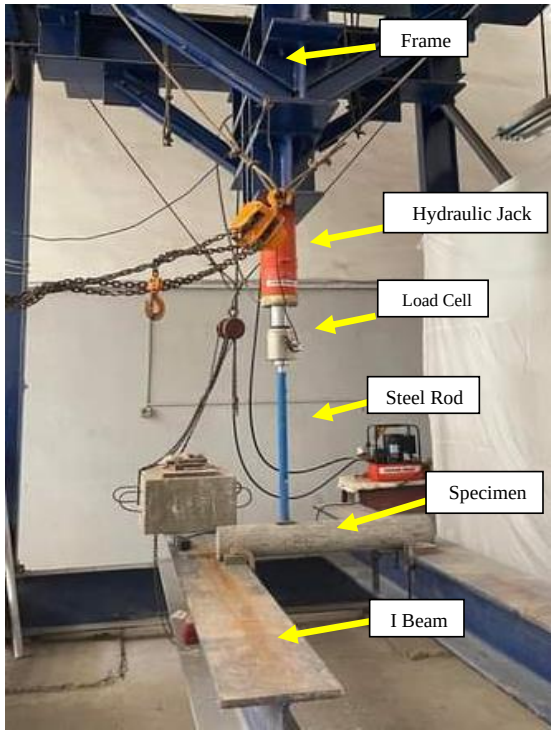

Fig. 3. Test Set-up.

3. Experimental Results and Discussion

3.1. Results For Ultimate Lateral Load and Displacement at Failure

Table 3 provides the Ultimate Lateral load (N), displacement at failure (mm), Reinforcement ratio (AS /AC) %, and the reinforcement cost (L.E.) for tested pile specimens Ps, Pc, Pl, PGA, PGB, PGC, PGD, PsGA, PsGB, PsGC, and PsGD.

Table 3. Summary of experimental results.

Group No.	Pile Code	Ultimate Lateral Load (N)	Ultimate Lateral Load/ load of Ps %	Displacement at Failure (mm)	Price of Reinforcement (L.E.)	Price of Reinforcement change to Ps
Reference	Ps	27853.1	100.0	11.30	40.00	-
First Group	Pl	33574.0	120.6	12.76	29.00	72.5
	Pc	29059.1	104.4	8.56	400.0	1000
Second Group	PGA	12205.5	44.0	5.44	6.10	15.2
	PGB	14627.6	53.0	3.98	11.40	28.5
	PGC	28356.8	101.8	12.51	16.40	41.0
	PGD	27880.6	100.1	26.82	19.00	47.5
Third Group	PsGA	21301.4	76.50	7.32	23.85	59.6
	PsGB	20959.5	75.30	8.11	29.15	72.8
	PsGC	34902.4	125.3	15.24	34.15	85.3
	PsGD	33684.6	120.9	12.98	36.75	91.2

3.2. Comparisons For Lateral Load Against Displacement

Fig. 4 illustrates the relationship between lateral load, and displacement for the experimented pile specimens Ps, Pc, and Pl. Also, the relationship between lateral load, and displacement for Ps, PGA, PGB, PGC, and PGD was shown in fig. 5. While the relationship between lateral load, and displacement for Ps, PsGA, PsGB, PsGC, and PsGD was shown in fig. 6. Finally, the relationship between lateral load, and displacement for Ps, Pl, Pc, PGA, PGB, PGC, and PGD was shown in Figs. (4-7).

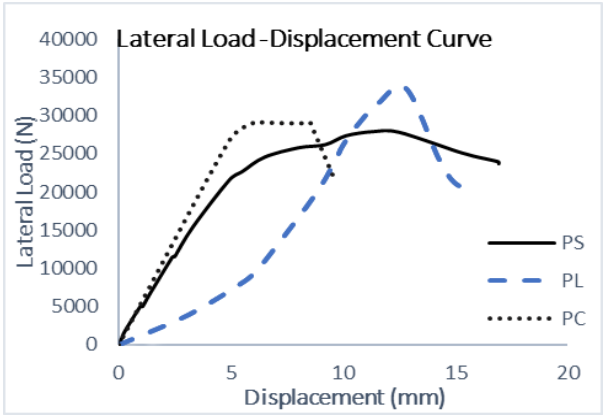

Fig. 4. The relation between the lateral load (N) and the displacement (mm) for tested pile samples Ps, Pc, and Pl.

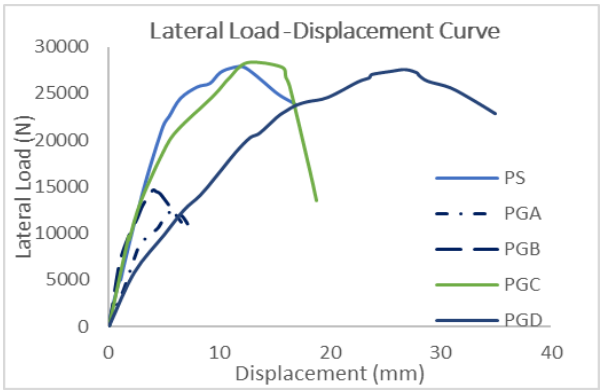

Fig. 5. The relation between the lateral load (N) and the displacement (mm) for tested pile samples Ps, PGA, PGB, PGC and PGD.

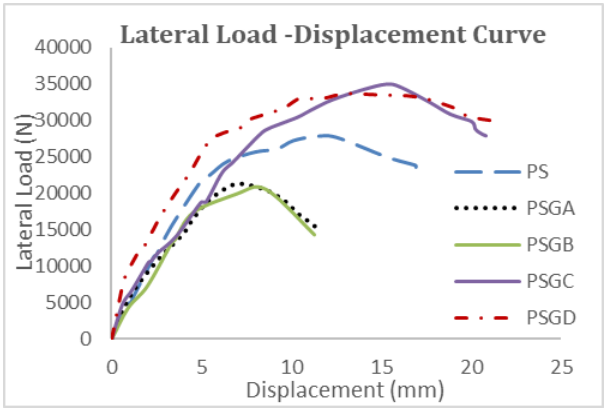

Fig. 6. The relation between the lateral load and the displacement for tested pile samples Ps, PsGA, PsGB, PsGC, and PsGD.

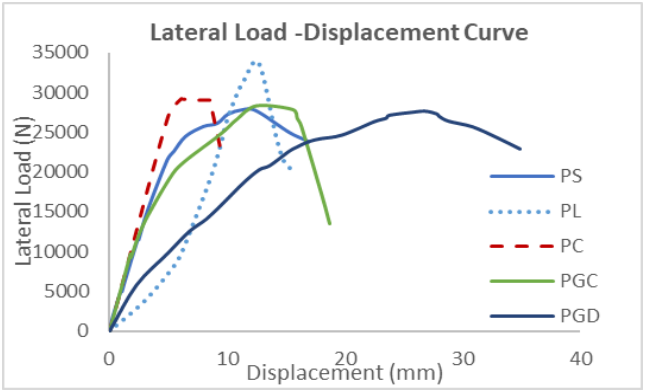

Fig. 7. The relation between the lateral load (N) and the displacement (mm) for tested pile samples Ps, Pl, Pc, PGC, and PGD.

3.3. Results and Discussion for Ultimate Lateral Load

The ultimate lateral loads for pile samples Pl, Pc, PGA, PGB, PGC, PGD, PsGA, PsGB, PsGC, and PsGD achieved a change of 120.6%, 104.4%, 44%, 53%, 101.81%, 100.1%, 76.5%, 75.3%, 125.31%, and 120.91% respectively compared to control pile sample (Ps) as shown in Table 3. As illustrated in fig. 8, the use of GFRP bars, CFRP bars, biaxial geosynthetic geogrid, or uniaxial geosynthetic geogrid resulted an increase in the ultimate lateral load from 0.1% to 25.31%. Conversely, the ultimate lateral load was decreased to 44%-53% of the control sample using triaxial geogrids. While it was decreased to 75.3% - 76.5% of the control pile sample using geogrid with a steel bar in the middle of the core.

Comparing the specimens reinforced with different bars material, the ultimate lateral load was successfully increased by 20.6% when GFRP bars were used instead of steel bars (Ps), and by 16.4% when CFRP bars were used (Pc), while it was increased relatively by 4.4% compared to control pile using CFRP bars as shown in fig. 4. The increase in ultimate lateral load of specimens reinforced with GFRP bars against CFRP bars was expected due to the high quality of the manufacturing process for GFRP bars.

Comparing the specimens reinforced with different geosynthetics geogrid materials as shown in fig. 9, it can be noted that the ultimate lateral load was increased to 1.81% by using biaxial geosynthetics geogrid and 0.1% using uniaxial geosynthetics geogrids. On the other hand, using triaxial geosynthetics geogrids (GA, GB) decreased the ultimate lateral load to 44%-53% of the control sample. The reason for this decrement was its ability to make confinement with low tensile strength.

Comparing the specimens reinforced with different geogrid materials with a steel bar in the middle of the core as shown in fig. 9, it can be noted that the ultimate lateral load was increased to 25.31% compared to the control pile using biaxial geosynthetics geogrid and 20.91% using uniaxial geosynthetics geogrids. On the other hand, it can be noted that the ultimate lateral load was increased using the triaxial geosynthetics geogrids GA compared to using GB.

The reinforcement cost for pile specimens Pl, PGA, PGB, PGC, PGD, PsGA, PsGB, PsGC, and PsGD was decreased to 72.5%, 15.2%, 28.5%, 41%, 47.5%, 59.6%, 72.8%, 85.3%, 91.2% compared to the control pile specimens.

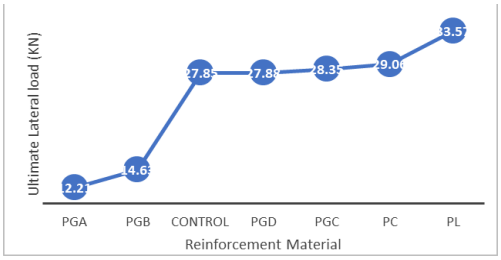

Fig. 8. The ultimate lateral load vs reinforcement material relationship at same reinforcement ratio.

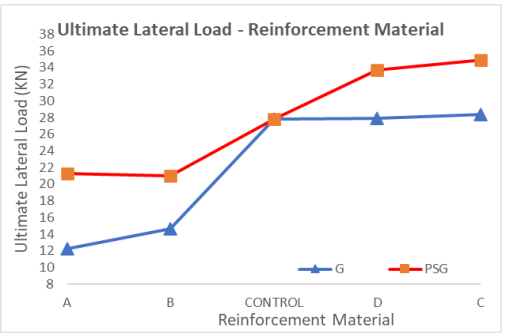

Fig. 9. Ultimate lateral load vs geosynthetics geogrids type with or without bar in the core.

3.4. Failure Modes

The failure mode for the control specimens was a ductile failure. Also, the failure modes for all samples reinforced by GFRP bars, triaxial, biaxial, uniaxial geosynthetics geogrids, or geosynthetics geogrids with bar in the middle of core were a ductile failure by tension while, the failure modes for all samples reinforced by CFRP bars were a brittle failure by tension. An observed sudden failure was happened during the test. The failure modes for all samples are shown in fig. 10.

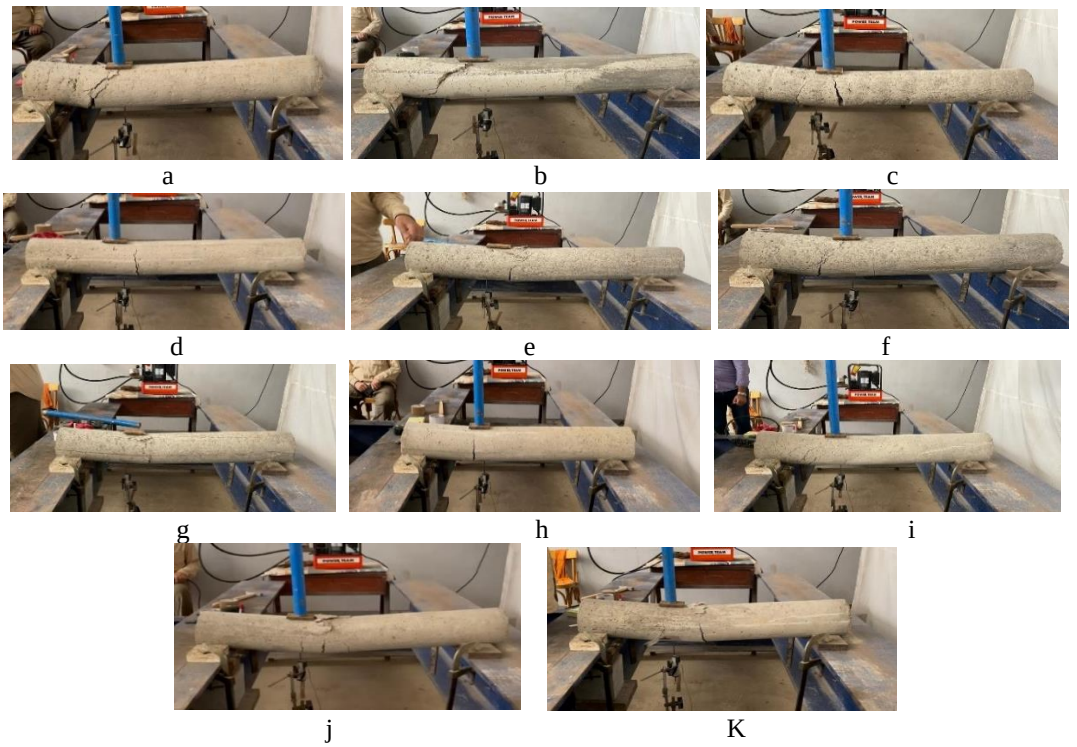

Fig. 10. Failure modes for samples a) Ps, b) Pl, c) Pc, d) PGA, e) PGB, f) PsGA, g) PsGB, h) PGC, i) PGD, j) PsGC, and k) PsGD.

4. Non-linear finite Element Analysis

4.1. Numerical Analyses

A nonlinear finite-element (F.E) analysis was performed using a finite-element software Abaqus/CAE standard 6.14-2 to simulate the normal behavior of circular concrete piles reinforced with steel bars, GFRP, CFRP, and geosynthetics geogrids under the effect of lateral load. A lot of factors were considered in the modeling such as, parts for the model, material properties, the assembly for the model, steps of the model, the interaction for the model parts, loading condition, mesh sensitivity then submission to solve the model. Concrete and reinforcing bars (steel, FRP and geosynthetics geogrids) were used in the current study to simulate the parts.

To accurately simulate the experimental work, the identical material properties applied in the experimental work for the concrete, steel, GFRP, CFRP bars, and geosynthetic geogrids (triaxial, biaxial, and uniaxial) were inputted into the Abaqus software to exactly reproduce the experimental work. The material properties factors were considered in modeling, such as compressive strength of concrete, yield stress and tensile strength of steel, tensile strength of FRP bars and geosynthetic geogrids also, modulus of elasticity of the materials of the reinforcement. A liner stress- strain curve was defined for the GFRP, CFRP, and steel bars as shown in fig. 11.

A 3D deformable solid parts were used to model the concrete circular pile and the ending plates. However, 3D deformable wire parts were used to model the reinforcement as steel, FRP bars and a 3D deformable shell planar part was used to model the geosynthetic geogrids shells. The reinforcement elements were inserted as embedded elements in the circular concrete pile part. four material types were used for the reinforcement such as steel, GFRP, CFRP, and geosynthetic geogrids (triaxial, biaxial, and uniaxial) to simulate the longitudinal bars. The total length of the circular concrete pile specimens was modeled. Also, two ring plates were modeled to confine the circular reinforced concrete pile specimens. The simulation of the reinforcement concrete pile was shown in fig.12.

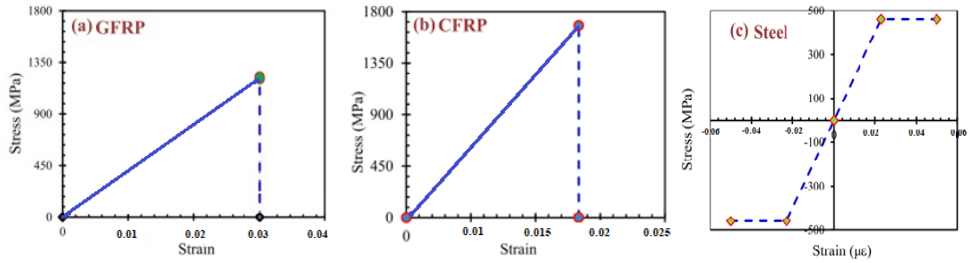

Fig. 11. Stress- strain curve of reinforcement material a) GFRP, b) CFRP, c) steel.

The Abaqus software generates nonlinear finite element models that contain thousands of variables. As a result, the applied load must be applied in steps to take advantage of the nonlinearity effect. At the ending of each load step, the program updates the solution

and applies it to the subsequent step. A series of little increments were used to create the solution, and each one was subsequently solved. For the purpose of numerically resolving the nonlinear equilibrium equations, Newton's method was selected as the solver. The real motive for this decision is the Newton's method's higher convergence rate when compared to other methods' convergence rates for the nonlinear issues that Abaqus is most generally used to study.

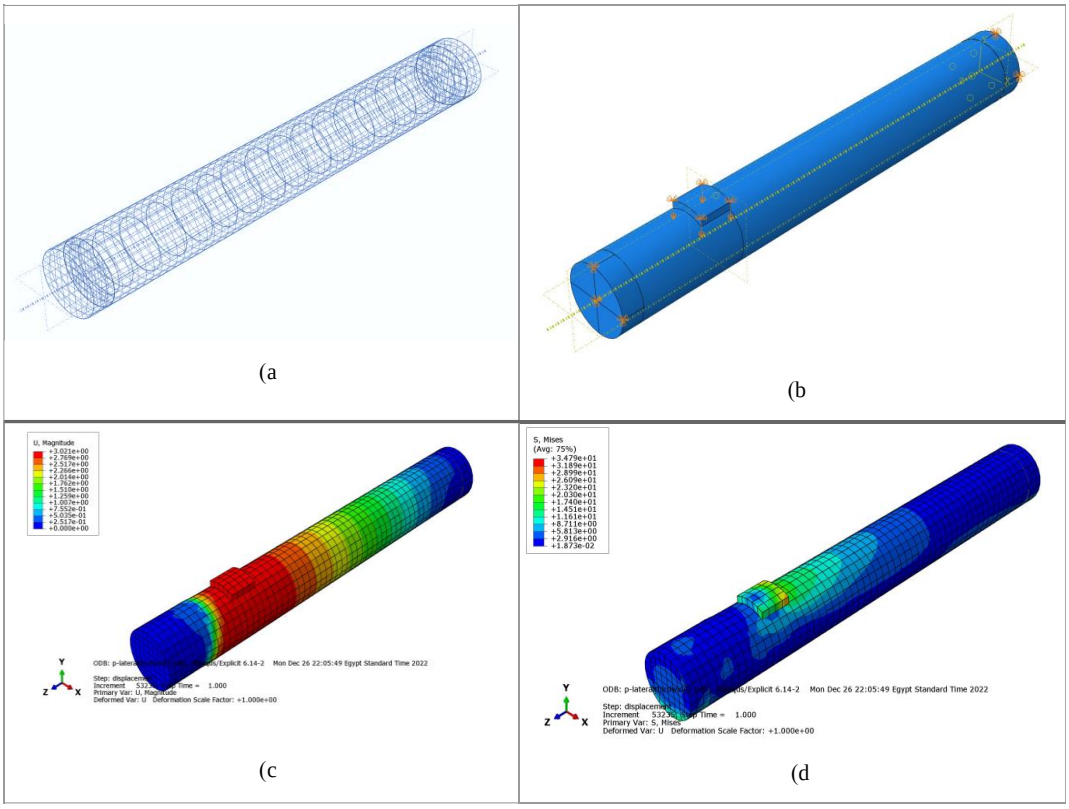

Fig. 12. Simulating of circular reinforcement concrete pile. a) Meshing of the elements, b) Case of loading (Lateral load), c) The displacement on the pile, d) Stresses on the pile.

The FEM was verified by comparing its output results with the results from previous studies. The model has been commonly used in the finite element modeling of the reinforced concrete pile by various researchers. For example: a model by (Ali, et. al, 2020) was successfully used for analyzing reinforced concrete piles to study the behavior of a reinforced concrete pile under shear force. The finite element model was verified using Abaqus/CAE standard 6.14-2 software. The failure load for Ali's concrete pile reaches 627 KN in the experimental result, while the failure load in this study reached 600 KN in the FEM results as shown in fig. 13. The results showed that the variation in results doesn't exceed 5%, and that is accepted, so this program could be used for different parameters which the study mentions as the following.

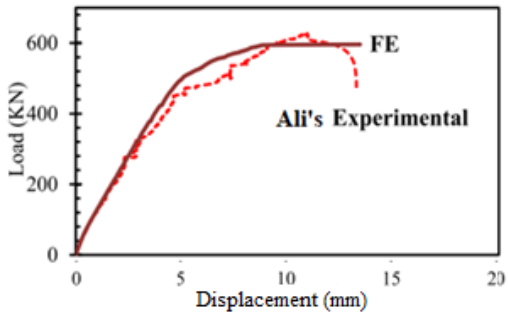

Fig. 13. Comparison between Ali's and FEM for Load- Displacement curve.

4.2. Results for Numerical Analyses

The results achieved by the FEM simulation were verified with the experimental results of the tested pile specimens. The FE model was used for the verification process of the pile specimens (Ps, Pl, Pc, PGA, PGB, PGC, PGD, PsGA, PsGB, PsGC, PsGD). The pile specimens Pl, Pc, PGA, PGB, PGC, PGD, PsGA, PsGB, PsGC, and PsGD achieved an increase in ultimate lateral load of 119.9%, 108.4%, 47.7%, 54.1%, 104.2%, 102.8%, 81.4%, 84.3, 129.9%, and 125.1% respectively compared to the control pile specimen Ps. Regarding the curve representing the lateral load-displacement, a comparison was established. In the FEM results, the test parameters included the modulus of elasticity of the reinforcement and the longitudinal reinforcement ratio. Steel, GFRP, CFRP bars and geogrid geosynthetics were used as reinforcing materials in FEM simulation such as in the experimental program. A comparison between the experimental, and FEM results was shown in table (4). The experimental, and the FEM ultimate lateral load results were shown in table (4) and achieved a great convergence as shown.

4.3. Comparison of Experimental, and FEM Results

Fig.14 shows the load-displacement curves for the experimental and FEM results of the selected piles, to show the effect of reinforcing material on the lateral load of circular reinforced concrete piles. The results illustrated that the finite element model was very accurately able to represent the load-displacement relationship of the experimental results. Also, the circular reinforced concrete pile specimen's displacement computed in the FEM and the displacement obtained experimentally are in good agreement with the experimental.

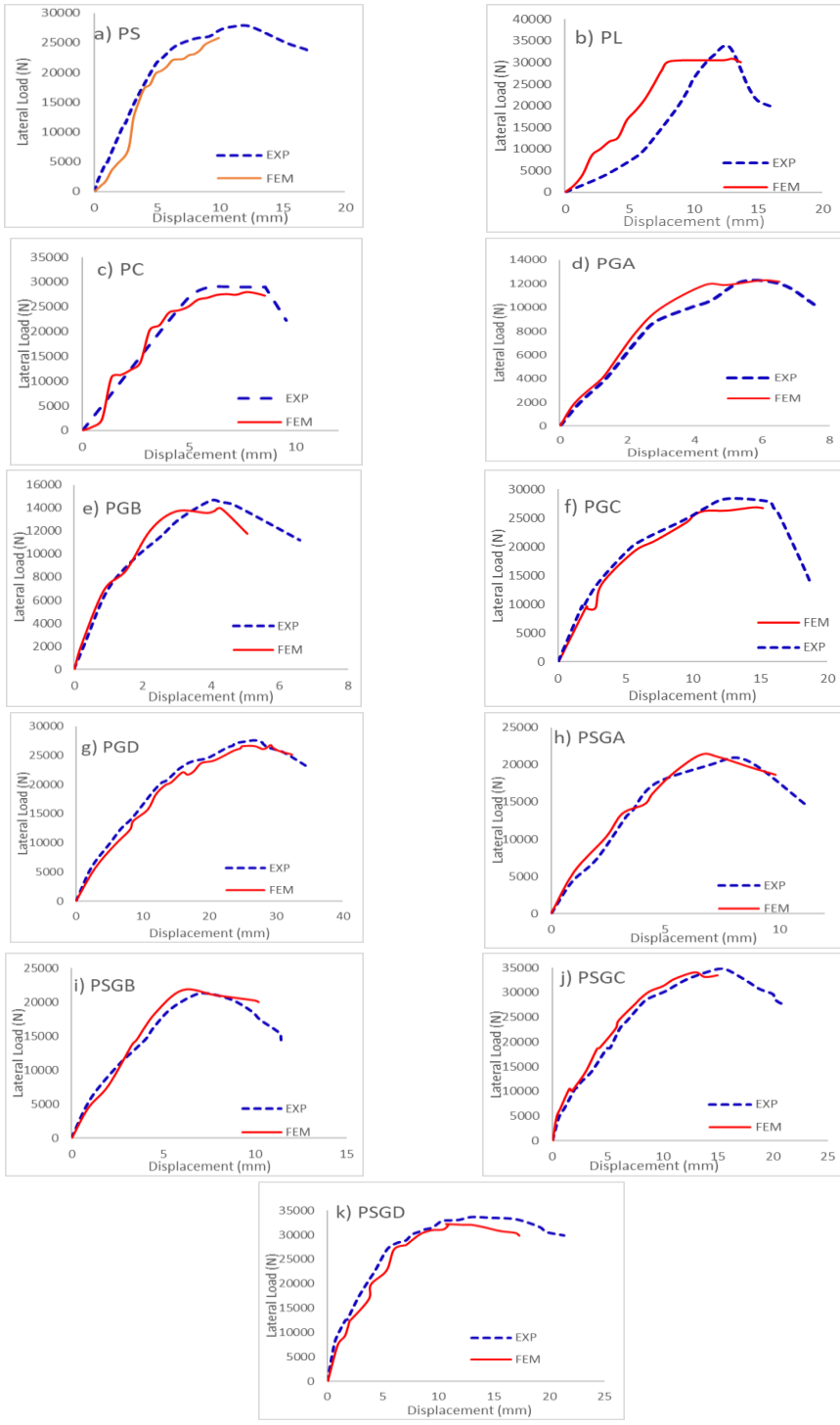

Fig. 14. Load–Displacement relationship for experimental and FEM.

Table 4. Experimental and FEM results.

Pile Code	Material	P_{EXP} (N)	P_{FE} (N)	P_{EXP} / P_{FE}
Ps	Steel	27853.1	25815.1	1.0789
Pl	Glass Fiber Bars (GFRP)	33574	30967.28	1.0842
Pc	Carbon Fiber Bars (CFRP)	29059.1	27993.23	1.0381
PGA	Triaxial Geogrids (GA)	12205.5	12312.1	0.991
PGB	Triaxial Geogrids (GB)	14627.6	13945.09	1.0489
PGC	Biaxial Geogrids (GC)	28356.8	26890.94	1.0545
PGD	Uniaxial Geogrids (GD)	27880.6	26554.15	1.049
PsGA	Triaxial Geogrid+Steel Bar	21301.4	21008.24	1.0139
PsGB	Triaxial Geogrid+Steel Bar	20959.5	21756.42	0.9634
PsGC	Biaxial Geogrids+Steel Bar	34902.4	33547.2	1.0404
PsGD	Uniaxial Geogrids+Steel Bar	33684.6	32280.4	1.0435
			Mean	1.037
			SD	0.0356
			Covariance	0.001269

5. The Effect of Simulating the Soil Surrounded the Pile Sample.

5.1. The Pile- Soil Simulation

A 3D non-liner finite element simulation was performed in the Abaqus standard software program to simulate Pile- Soil analytical model, as shown in fig. 15. A pile surrounded with soft clay soil and rested on crushed stones layer was performed in the simulation. A 3D deformable solid part was used to model the crushed stones layer, concrete pile, and loading plate. While a 3D deformable wire element was used to model the steel longitudinal bars and transverse hoops. The reinforcement was modelled as an embedded elements within the concrete element. The soil properties used in the FEM were illustrated in Table 5. A liner elastic stress- strain curve was specified for the steel bars. The total length of the concrete pile specimen was simulated. To simulate the boundary condition under the load, a degree of freedom was allowed to simulate the actual condition between the pile and the pile cap. A surface-to-surface contact has occurred between the soil and the pile, and the pile was performed as an explicit body.

Table 5. The properties of the soil used**.**

Type of soil	Modulus of elasticity (MPa)	Poisson's ratio	Friction angle (^{o})	Cohesion (KPa)
Very soft clay	15	0.15	0	12
Crushed stone	100	0.5	40	0

5.2. FEM Results for Simulating the Soil Around the Pile Sample.

The result gained from the FEM simulation for the pile- soil analytical model (with soil around the pile) was verified against the result obtained from the FEM simulation for the Pile analytical model (without soil around the pile). The results of FEM ultimate lateral load for the pile-soil and the pile model were 27.1 KN and 25.8 KN respectively. The results showed good convergence with and without simulating the soil in the analytical model by 5%. According to, the 3D non-linear finite element simulation performed in the Abaqus standard software program the effect of soft clay soil surrounding the pile was neglected in the experimental cases.

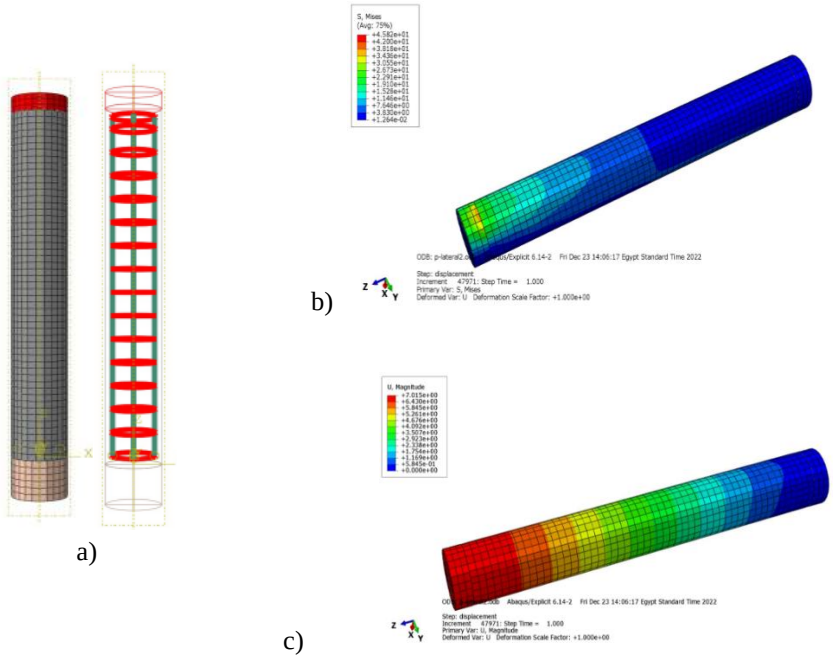

Fig. 15 Simulation of circular reinforcement concrete pile in soft clay soil and rested on crushed stones soil. a) meshing and reinforcement of the pile, b) Stresses on the pile, c) Displacement on the pile.

6. Conclusion

- Using FRP bars, biaxial or uniaxial geosynthetics geogrids as reinforcement enhanced the ultimate lateral load of the pile compared to the control sample, which destructed in a ductile tension failure mode.
- The ultimate carried lateral load of pile was increased for samples reinforced with biaxial and uniaxial geosynthetics geogrids with or without a steel bar in the middle of core,
- The ultimate carried lateral load of pile was decreased for samples reinforced with triaxial geosynthetics geogrids with or without and steel bar in the middle of core, but

the bar placed in the middle of the core was effective in carrying lateral load with the geosynthetics geogrids.

- The cost of the reinforcement was decreased effectively for the pile specimens reinforced by GFRP bars or geosynthetics geogrids (triaxial, biaxial, uniaxial).
- A sudden brittle failure was occurred, for all samples reinforced by CFRP bars, While A ductile failure by compression was happened for all samples reinforced by geogrid with or without a steel bar in the middle of core.
- Non-linear finite Element analysis has been verified and achieved a great convergence against the experimental results.

7. References

[1] E. Guades, T. Aravinthan, M. Islam, and A. Manalo, "A review on the driving performance of FRP composite piles," Compos Struct, Elsevier, vol. 94, pp. 932–1942, 2012.

[2] K. E. Kim, and B. Andrawes, "Compression behavior of FRP strengthened bridge timber piles subjected to accelerated aging," Construction and Building Materials, Elsevier, vol. 124, pp. 177-185, 2016.

[3] K. Zyka, and A. Mohajerani, "Composite piles: A review," Construction and Building Materials, Elsevier, vol. 107, pp. 394–410, 2016.

[4] M. G. Iskander, A. Stachula, "Wave equation analyses of fibre-reinforced polymer composite piling," J Compos Constr., vol. 6, pp. 88–96, 2002.

[5] A. Z. Fam, S. H. Rizkalla, "Flexural behaviour of concrete-filled fibre-reinforced polymer circular tubes," J Compos Constr, vol. 6, pp. 123–32, 2002.

[6] M. Sakr, M. H. Naggar, M. Nehdi, "Load transfer of fibre-reinforced polymer (FRP) composite tapered piles in dense sand," Can Geotech J, vol. 41, pp. 70–88, 2004.

[7] H. Zhang, and M. S. Hadi, "Geogrid-confined pervious geopolymer concrete piles with FRP-PVC confined concrete core: Concept and behaviour," Construction and Building, Elsevier, Materials, vol. 211, pp.12–25, 2019.

[8] M. Sakr, M. H. El-Naggar, and M. Nehdi, "Interface characteristics and laboratory constructability tests of novel fibre-reinforced polymer/concrete piles," J Compos Constr, vol. 9, pp. 274–83, 2005.

[9] T. Mukhopadhyay, S. Naskar, P. K. Karsh, and S. Dey, "Effect of delamination on the stochastic natural frequencies of composite laminates," Comp. Part B, vol. 154, pp. 242–256, 2018.

[10] A. H. Ali, B. Mohamed, and A. El-Safty, “Effect of applied sustained load and severe environments on durability performance of carbon-fiber composite cables (CFCCs),” J Compos Mater, vol. 53, pp. 1–16, 2018.

[11] T. Mukhopadhyay, S. Naskar, S. Dey, and S. Adhikari, “On quantifying the effect of noise in surrogate based stochastic free vibration analysis of laminated composite shallow shells,” Compos Struct, Vol. 140, pp. 798–805, 2016.

[12] T. Mukhopadhyay, S. Naskar, S. Dey, and A. Chakrabarti, “Condition Assessment and Strengthening of Aged Structures: Perspectives Based on a Critical Case Study,” Practice Periodical on Structural Design and Construction, vol. 24, Issue 3, 2019.

[13] M. G. Iskander, M. Hassan, “State of the practice review in FRP composite piling,” J Compos Constr., vol. 2, pp. 116–20, 2002.

[14] M. A. Pando, C. D. Ealy, G. M. Filz, J. J. Lesko, and E. J. Hoppe, “A laboratory and field study of composite piles for bridge substructures,” Office of Infrastructure R&D, Federal Highway Administration, 6300 Georgetown Pike, McLean, 2006.

[15] C. S. Sirimanna, “Behaviour of fibre composite piles for timber pile rehabilitation,” Master of engineering dissertation, University of Southern Queensland, Toowoomba, Queensland, Australia, 2011.

[16] E. J. Guades, T. Aravinthan, and M. M. Islam, “Driveability of composite piles,” In: Proceedings of the 1st intl postgraduate conference on eddBE2011, Brisbane, Australia, 2011, pp. 237–42.

[17] J. Giraldo, and M. T. Rayhani, “Load transfer of hollow Fiber-Reinforced Polymer (FRP) piles in soft clay,” Elsevier, Transportation Geotechnics, vol. 1, pp. 63–73, 2014.

[18] A. H. Ali, A. Goudaa, H. M. Mohameda, M. H. Rabiea, B. Benmokraneb, “Nonlinear finite elements modeling and experiments of FRP-reinforced concrete piles under shear loads,” Structures, Elsevier, vol. 28, pp. 106-119, 2020.

[19] ECP-Egyptian Code of Practice-201, "Egyptian code of practice" no. 201 for calculating loads and forces in structural work and masonry, National Research Center for Housing and Building, Ministry of Housing, Utilities and Urban Planning, Cairo, 2011.

[20] Armastek and imported by Fiber Reinforcement Industries Company, Baku, Khazar district 2-km Highway Gala Pirallahi 3B, youremail@website.com, web. https://armastek.az/en/home-page/.

[21] Sika Company, 1st industrial zone (A) Section # 10, Block 13035 El-Obour City, Egypt, Tel. +202-44811014, Fax. +202-44810459, web. https://egy.sika.com/.

[22] Tensar International Corporation and imported, 2500 Northwinds Parkway, Suite 500 Alpharetta, GA 30009, Tel. (770) 344-2090 Email: info@tensarcorp.com, web. https://www.tensarcorp.com/solutions/geogrids/triax.

[23] Degla Co. For Import & Export, 1 Street 199, Maadi as Sarayat Al Gharbeyah, Maadi, Cairo, Tel**:** 02 25241054, web. https://degla.co.